Author Manuscript

Author Manuscript

Author Manuscript

Author Manuscript

HHS Public Access

Author manuscript

J Neurosci Methods. Author manuscript; available in PMC 2017 January 30.

Published in final edited form as:

J Neurosci Methods. 2016 January 30; 258: 46–55. doi:10.1016/j.jneumeth.2015.10.007.

Two-photon imaging of chronically implanted neural electrodes: Sealing methods and new insights

Takashi D. Y. Kozai[1,2,3,4], **James R. Eles**[1,2], **Alberto L. Vazquez**[1,2,5], and **X. Tracy Cui**[1,2,3]

[1] Bioengineering, University of Pittsburgh.

[2] Center for the Neural Basis of Cognition, University of Pittsburgh.

[3] McGowan Institute for Regenerative Medicine, University of Pittsburgh.

[4] NeuroTech Center of the University of Pittsburgh Brain Institute

[5] Radiology, University of Pittsburgh

Abstract

Background—Two-photon microscopy has enabled the visualization of dynamic tissue changes to injury and disease *in vivo*. While this technique has provided powerful new information, *in vivo* two-photon chronic imaging around tethered cortical implants, such as microelectrodes or neural probes, present unique challenges.

New Method—A number of strategies are described to prepare a cranial window to longitudinally observe the impact of neural probes on brain tissue and vasculature for up to 3 months.

Results—It was found that silastic sealants limit cell infiltration into the craniotomy, thereby limiting light scattering and preserving window clarity over time. In contrast, low concentration hydrogel sealants failed to prevent cell infiltration and their use at high concentration displaced brain tissue and disrupted probe performance.

Comparison with Existing Method(s)—The use of silastic sealants allows for a suitable imaging window for long term chronic experiments and revealed new insights regarding the dynamic leukocyte response around implants and the nature of chronic BBB leakage in the sub-dural space.

Conclusion—The presented method provides a valuable tool for evaluating the chronic inflammatory response and the performance of emerging implantable neural technologies.

Corresponding authors: Takashi D.Y. Kozai, Ph.D., Department of Bioengineering, University of Pittsburgh, 208 Center for Bioengineering, 300 Technology Dr., Pittsburgh, PA 15219, tdk18@pitt.edu, X. Tracy Cui, Ph.D., Department of Bioengineering, University of Pittsburgh, 5057 Biomedical Science Tower 3, 3501 Fifth Avenue, Pittsburgh, PA 15260, Ph: 412-383-6672, Fx: 412-648-9076, xic11@pitt.edu.

Publisher's Disclaimer: This is a PDF file of an unedited manuscript that has been accepted for publication. As a service to our customers we are providing this early version of the manuscript. The manuscript will undergo copyediting, typesetting, and review of the resulting proof before it is published in its final citable form. Please note that during the production process errors may be discovered which could affect the content, and all legal disclaimers that apply to the journal pertain.

Author Manuscript Author Manuscript Author Manuscript Author Manuscript

Keywords

Foreign Body; Giant Cell; intracortical microelectrode; intravital imaging; reactive tissue response; encapsulation; Multiphoton

Introduction

Implantable intracortical electrodes are powerful neuroscience research tools that allow investigators to link low level neural circuits to behavior, decision making, memory, learning, and the progression of neurological injury and disease (Gage et al., 2010; Ganguly and Carmena, 2009; Guitchounts et al., 2013; Kozai et al., 2015c; Stoetzner et al., 2010). More recently, they have demonstrated significant promise in restoring functional control to patients with tetraplegia by extracting the intent of the subject via detection of firing rates of small populations of neurons (Collinger et al., 2012; Hochberg et al., 2012). Despite these promising results, large inter-animal and intra-animal variability in device performance have limited its usefulness in potential applications(Freire et al., 2011; Kozai et al., 2015b; Kozai et al., 2015c; Kozai et al., 2014c; Ludwig et al., 2006; Rousche and Normann, 1998; Saxena et al., 2013; Williams et al., 1999).

The unpredictable nature of recording failure is hypothesized to be due to the combination of the inflammatory response and material failure over time following implantation (Barrese et al., 2013; Kozai et al., 2015b; Kozai et al., 2015d; Kozai et al., 2014c; Kozai et al., 2010; Prasad et al., 2012) (see (Kozai et al., 2015d) for Review). For example, material failure is believed to range from recording site to insulation damages including delamination, crack propagation, hydration which leads to loss of dielectric properties and iconic contamination (Escamilla-Mackert et al., 2009; Gilgunn et al., 2013; Kim et al., 2014; Kozai et al., 2014a; Kozai et al., 2015a; Kozai et al., 2015b; Prasad et al., 2014; Prasad et al., 2012; Sankar et al., 2014; Ware et al., 2014). On the other hand, biological failure modes are believed to be due to the inflammatory reactive tissue response to the implanted electrode (Gilgunn et al., 2012; Jaquins-Gerstl et al., 2011; Karumbaiah et al., 2012; Kozai et al., 2014a; Kozai et al., 2014b; Kozai et al., 2012a; Kozai et al., 2014c; Kozai et al., 2010; Potter et al., 2013; Rennaker et al., 2007; Turner et al., 1999). Unlike material failure modes of implantable electrodes(Kozai et al., 2015b; Prasad et al., 2012; Stensaas and Stensaas, 1978), the mechanism(s) behind the progression of the tissue response and the large variability of observed outcomes are poorly understood (Kozai et al., 2015d).

Complex feedback and feedforward biochemical pathways involved in the tissue response makes it difficult to identify cause and effect relationships, especially from post-mortem histology. For example, BBB disruption can lead to inflammation and neural degeneration, but neural degeneration from hypoxia can also induce BBB leakage (Kozai et al., 2015d). Furthermore, recent studies examining the relationship of postmortem histology to the recording performance of nearby recording sites demonstrated the poor predictability of post-mortem tissue to actual recording performance (Kozai et al., 2014c). Similarly, *in vivo* electrochemical impedance spectroscopy suffer from challenges in disentangling the multiple biological and material causes that lead to recording failure (Kozai et al., 2015b).

Author Manuscript Author Manuscript Author Manuscript Author Manuscript

These studies show that these evaluation metrics lack the spatiotemporal resolution for identifying cause and effect relationships that lead to the larger discrepancies between high performing implants and rapidly failing implants.

In vivo two-photon microscopy (TPM) is an emerging technique for studying the progression of biological processes in tissue beyond the depth range of conventional confocal microscopy and resolution beyond photoacoustic imaging, magnetic resonance imaging, or fluorescence molecular tomography. TPM has been successfully used as a research tool to understand temporal dynamics of injury and disease (Bell et al., 2010; Davalos et al., 2005; Kozai et al., 2012b; Masamoto et al., 2012; Wake et al., 2009) For example, *in vivo* TPM has been previously used to map the BBB prior to implant insertion (Kozai et al., 2010). This mapping technique identified regions in the cortex where large blood vessels penetrate into the cortex as well as regions densely filled with small capillaries, which are only wide enough to allow a single blood cell to pass at time. This study showed that severing a large arteriole in Layer III led to significantly greater intracranial hemorrhage compared to penetrating through dozens of small capillaries. This, in turn, may be a potential source of the performance variability reported in recent studies (Prasad et al., 2014; Saxena et al., 2013).

More recently, TPM has been conducted with transgenic animals to study the dynamic changes of specific cell types immediately following implant insertion. In these acute preparations, microglia have been observed polarizing towards the implant surface and occasionally to nearby injured BBB by extending their processes and initializing encapsulation with lamellipodia sheaths (Kozai et al., 2012b). It was also shown that neurons adjacent to implanted devices become compressed due to the increased tissue strain from the volumetric tissue displacement from probe insertion (Kozai et al., 2014c). Although these studies have provided essential insight, this acute preparation is limited by the animal's viability following prolonged exposure to anesthesia, which typically ranged in reliability between 7-8 hrs up to 17 hrs. Therefore, in order to image and track long term changes around the implant it is necessary to develop methods for longitudinal imaging over weeks and months.

Here we report the method used to longitudinally image the tissue interface around chronically implanted intracortical electrodes for up to 12 weeks. Several strategies for improving recovery and longitudinal imaging are described and discussed. In summary, filling the craniotomy/coverslip window with aCSF leads to infiltration of $CX3CR1^{+}$ cells and giant cells that cause light scattering and reduce imaging depth. Using *in situ* forming PEG hydrogels holds the promise of low cell invasion while achieving optimal curing time and desired mechanical properties for a craniotomy sealant. However, the high concentration gel swells in the epidural space, compressing the tissue down and away from the electrode. Low concentration hydrogels such as alginate do not swell as much but can form scaffolds for cell infiltration and growth, as often employed in 3D cell cultures (Tibbitt and Anseth, 2009). Finally, filling the craniotomy with fast curing silicone reduces the cell infiltration, though this appears to depend on the amount of brain herniation when the coverslip window is sealed. This is the first step towards a more precise spatiotemporal understanding of the dynamic cellular response to implanted arrays over days and weeks. This method was used

Author Manuscript Author Manuscript Author Manuscript Author Manuscript

to report novel observations at the brain-machine interface including cellular infiltration and new insights to chronic BBB leakage. These findings further highlight avenues for improving the chronic two-photon imaging window and understanding the macroscopic tissue health near the implant.

Methods

Two types of chronically implanted intracortical electrodes were used in this work: 1) CM style four-shank 3 mm long Michigan silicon electrodes with 177 μm^2 iridium recording sites on 15 μm thick by 100 μm wide shanks, and 125 μm center-to-center shank spacing (Neuronexus Technologies, Ann Arbor, MI) or 2) custom three-shank 1.5mm long Utah silicon electrodes (Blackrock Microsystems, Salt Lake City, UT). The electrodes were implanted into the cerebral cortex of eight wild-type mice (C57BL6J: Jackson Laboratories; Bar Harbor, ME) and eight transgenic mice (22-30g) that express green fluorescent protein (GFP) in leukocytes under the direction of the CX3CR1 promoter (CX3CR1-GFP: Jackson Laboratories; Bar Harbor, ME). The animals were induced with an anesthetic mixture consisting of 75 mg/kg ketamine and 7 mg/kg xylazine administered intraperitoneally. When necessary, the anesthetic plane was maintained with regular Ketamine updates of 40 mg/kg every 45 min or as needed by monitoring heart rate. After induction, the animal was placed in a stereotaxic frame, and the skin and connective tissue on the surface of the skull was removed. A thin layer of Vetbond (3M) was placed over the skull to help dry the bone and improve adhesion to the imaging well. Three or four bone screw holes were made using a high-speed dental drill over both motor cortex and the edges of visual cortex (Fig. 1a-c). After the bone screws were put in (1.5 to 2 turns), a 3 sided 1–1.5 mm tall well was constructed around the edges of the skull using dental cement (Fig. 1d). A 4 mm by 6 mm craniotomy was made by thinning the skull around the somatosensory and visual cortex using a high-speed dental drill (Fig. 1e). The skull was periodically bathed in saline to ensure that the underlying cortex did not experience thermal damage from drilling. Care was taken to prevent vascular damage during drilling and the removal of the bone. Electrodes were implanted following this preparation and the impact of different chronic window preparation strategies for longitudinal imaging using two-photon microscopy was assessed. End point histology was performed for verification of the two-photon imaging findings between 7 days to 3 months post-implantation.

All experimental protocols were approved by the University of Pittsburgh, Division of Laboratory Animal Resources and Institutional Animal Care and Use Committee in accordance with the standards for humane animal care as set by the Animal Welfare Act and the National Institutes of Health Guide for the Care and Use of Laboratory Animals.

Electrode Implantation

The electrode was positioned at a 30° angle from horizontal for insertion using a stereotaxic micromanipulator (Fig. 1f). Preliminary placement over the cortex and away from major vasculature was verified. After alignment, probes were inserted using a z-axis automated microdrive (MO-81, Narishige, Japan) at 100 μm/s for 500 μm such that the tip of the

Author Manuscript Author Manuscript Author Manuscript Author Manuscript

electrode was approximately 200–250 μm(~ layer 3) below the surface of the brain. Little or no bleeding was observed during insertion.

Longitudinal Imaging Window Preparation

The craniotomy was filled with either 1) aCSF, 2) cross-linked PEG hydrogel, 3) 1% agarose, or 4) Kwik-Sil before placing a glass coverslip and securing the glass coverslip and electrode with blue light curing dental cement. When sealing the craniotomy and glass coverslip with aCSF, a small air bubble was intentionally left to prevent chronic leakage from the chamber due to increased CSF pressure while the dental cement seal cured. Small air bubbles were naturally solubilized into the CSF solution and disappeared within 12 hours.

Low (10%) and high (30%) cross-linked poly(ethylene) glycol (PEG) were used to examine tradeoffs in curing speed and to minimize cellular infultration. *In situ* cross-linking of PEG based hydrogels were formed via Michael addition in a 1:1 ratio of 4-arm vinylsulfone end-functionalized PEG (10 kDa, Jenkem Technologies USA) and bifunctionalized thiol PEG (5 kDa, Jenkem Technologies USA) (Lutolf and Hubbell, 2003). Low concentration 10% PEG solutions cured slowly (>8 minutes) and were easily torn with mechanical manipulation. 30% PEG solutions thickened within 1 minute and achieved full gelation in less than 5 minutes. Because of the easy handling afforded by rapid gelation as well as the improved mechanical stability of a higher density gel, the 30% PEG gels were selected for *in vivo* testing. Once mixed, PEG solution was placed onto the exposed cortex until it sufficiently covered the craniotomy site.

Kwik-Sil was carefully placed into the craniotomy avoiding any air bubbles using the provided mixing tips. The coverslip was quickly placed over the Kwik-Sil while avoiding air bubbles and gently pressed to the skull. Excess Kwik-Sil was wiped away using an absorbent spear, and the edges of the coverslip were swiftly sealed using blue light curing dental cement.

The reliability of each strategy was evaluated by two-photon imaging and immunohistochemistry. Two-photon imaging was used to track the number of CX3CR1+cells in the craniotomy space as well as the vascular integrity.

Two-photon imaging

A two-photon laser scanning microscope was used for in vivo imaging. The microscope consisted of a scan head (Prairie Technologies, Madison, WI) and a Ti:sapphire laser (Mai Tai DS; Spectra-Physics, Menlo Park, CA) providing 100 fs pulses at 80 MHz tuned to a wavelength of 900 nm for this study. Fluorescence was detected using non-descanned photomultiplier tubes (Hamamatsu Photonics KK, Hamamatsu, Shizuoka, Japan) in whole-field detection mode using a 16X, 0.8 numerical aperture water immersion objective lens (Nikon Instruments, Melville, NY). Images with size of 1024 × 1024 pixel (815 × 815 μ m) were acquired every ~4.8 s per section using Prairie View software at ~20 mW (never exceeding 40 mW). The imaged volume was determined considering the desired image resolution, shank spacing, and inter-stack interval. Stacks were acquired along depth (Z

Author Manuscript Author Manuscript Author Manuscript Author Manuscript

stacks) every 3 μm at the following intervals; 12 h 24 h, 36 h, 48 h, 3 d, 4d, 5d, 6d, 7d, and once a week there after. For chronic imaging, animals were anesthetized with 1.2% isoflurane with 1L/min O_2 flow before being placed into the stereotaxic frame for imaging.

Immunohistochemistry

Between 2 weeks and 3 months, animals were deeply anesthetized with a 75 mg/kg ketamine and 7 mg/kg xylazine cocktail before being transcardially perfused with PBS followed by 4% paraformaldehyde. Dental cement headcaps were gently removed from the skull along the implant direction and allowed to post-fix in 4% paraformaldehyde (< 24 hours). Explanted headcaps were removed with glass coverslips, sealant, and neural probes still embedded within the dental cement. After washing in PBS, headcaps were blocked for 30 minutes in sodium citrate buffer (0.1M citric acid, 0.1M sodium citrate, pH 6.0) at room temperature followed by a peroxidase block (10% methanol, 3% hydrogen peroxide) for 20 minutes at room temperature on a shaker. Then, samples were blocked in a serum containing blocking buffer (5% normal goat serum, Jackson Labs; 0.1% Triton X-100, Sigma) for one hour, and incubated in primary antibodies directed to either monocytes (Iba-1, 1:500, Fisher), reactive monocytes (ED-1, 1:500, AdB Serotec), and/or fibroblasts/monocytes (Vimentin, 1:250, Millipore) for 12-24 hours. Following washes in phosphate buffer saline (PBS), tissue was incubated in 1:250 Alexa Fluor 488, 568 and/or 633 (Invitrogen) for 2 hours at room temperature, followed by more PBS washes, 10 minute incubation in 1:1000 dilution of Hoescht 33342 (Invitrogen) stain, and PBS washes. Samples were imaged with TPM as described above or Olympus Fluoview 1000 confocal scanning microscope with a 10X air immersion lens.

Results and Discussion

Microelectrodes were implanted into the mouse cortex and chronically fixed under an imaging window (Fig. 1). The impact of different imaging window preparations on reliable data acquisition from 7 days to 3 months was assessed. Several key issues were noted in engineering the window that enables long term imaging of the tissue. When combined with transgenic animal models, tracking of specific cell types around chronically implanted electrodes can be achieved. This enabled real time observation of the tissue around implants and revealed new dynamic information that has previously eluded electrochemical impedance spectroscopy and post-mortem immunohistochemical analysis.

Craniotomy

PEG hydrogels rapidly formed *in situ*, with similar curing time and mechanical stability as Kwik-Sil (<5 min). As soon as the craniotomy was sealed, the hydrogel absorbed CSF and expanded. This expansion compressed the cortex down and pushed it away from the electrodes (Fig. 2a). This tissue expansion was similar to those observed with dissolving insertion shuttles (Kozai et al., 2014b). By twelve hours post implant, the hydrogel had sufficiently expanded to completely compress away the tissue from the electrode. In one animal, this expansion generated sufficient pressure to break off two shanks from the probe base. In contrast, low density hydrogels such as 1% agarose hydrogels did not show

Author Manuscript Author Manuscript Author Manuscript Author Manuscript

noticeable expansion. The aCSF and silicone filled craniotomies showed clarity in imaging quality over the first 48 hours (Fig. 2bc).

Following the craniotomy, it is necessary to re-seal the resected bone in order to re-establish intracranial pressure and a more normal brain environment. A glass coverslip was used for this purpose while maintaining clear access to the brain for imaging. A challenge of this procedure is to perform it carefully without disturbing the implanted probe (without damaging the probe or exacerbating the implanted tissue by bumping the probe). Failure to swiftly seal the coverslip with dental cement generally leads to leaks along the window and the dental cement interface due to the increasing presence of CSF fluid.. One approach is to seal along the window save one or two small holes (to be filled at the end), and then a small amount of aCSF can be removed with an absorbent spear. Leaving a small air pocket during the sealing procedure can help in forming an airtight seal. The air bubble likely acts as a buffer while the dental cement is curing, since gas is able to undergo volumetric change to compensate for increase in CSF pressure. More importantly, small air bubbles under the coverslip are solubilized into the CSF over the course of several hours. By placing these air bubbles at a distance away from the imaging region of interest, scanning of the tissue around the probe can be initiated immediately. With Kwik-Sil, the challenge is to avoid generating any air bubbles in the silastic while avoiding damaging the tissue by bumping the electrode during the installation of the window before the silicone cures.

Early Chronic Imaging—By 1 week post-implantation, CX3CR1^{+} cells were generally found in all of the cranial windows, which reduced the imaging depth from ~600 μm on the day of the implantation to about 300 μm. Cell migration to the CSF space below the craniotomy was found to be substantial in all preparations where the craniotomy was filled with aCSF (n=5; Fig. 3a). Substantial cell accumulation to the glass cover slip on the proximal surface ot the tissue was observed. Similarly, low density hydrogels provided cells with a scaffold for greater cell infiltration into the craniotomy space which led to a rapid initiation of bone regrowth on the order of 1-4 wks (n=4; data not shown). Cell infiltration into this space was reduced by using the fast curing two part silicone elastomer, Kwik-Sil (a transparent version of Kwik-Cast) in all animals (n=6; Fig. 3b). When using fast curing silicone it was important to consider anesthesia and its potential impact on brain herniation. For example, Isoflurane is a popular inhalant anesthesia, but it is also a vasodilator. As a result, this will generally lead to brain herniation during surgery, which the silicone will mold to. Once the craniotomy is sealed and the animal is recovered, the tissue will return to its original size, resulting in a large gap between the molded silicone surface and the brain surface. Moreover, this often led to bone formation below the silicone elastomer in longer term chronic time points (1-3 months). Therefore, ketamine/xylazine anesthesia was preferred.

While these CX3CR1^{+} cells are relatively transparent and difficult to see under a bright field surgical microscope, they scatter light and significantly reduce the imaging depth of the two-photon imaging system. This is likely due to the difference between single-photon optics and two-photon optics, as well as CCD and PMT detectors. Although the clarity in bright field images of the brain surface mirror clarity in deep multiphoton images in classical window preparations without penetrating electrodes, the presence of a chronically implanted

Author Manuscript Author Manuscript Author Manuscript Author Manuscript

device combined with the full craniotomy may contribute to the apparent non-linear effects on clarity. For this reason, in many two-photon neuroscience studies, recent emphasis has been placed on employing thin skull preparations to avoid infiltration of inflammatory cells. However, for understanding the tissue response around implantable neural electrodes, a thin skull preparation is not adequate. The results presented here show that the injury resulting from the craniotomy and the tissue reaction to the headcap play a role in the tissue response to the underlying brain around the implant and must be studied together. Current neural probe implantations in long term neurophysiology research and clinical neural interface applications require full craniotomies. As such, to mimic the situation, it is pertinent to study the tissue reaction associated with the electrode with full craniotomy.

CX3CR1+ Cells—CX3CR1+ cells not only accumulated in the craniotomy area, they also adhered to glass, silicone elastomers, and probes in all animals. This accumulation was lowest in animals where the silicone sealant was used. They can migrate to the window several microns per minute (Fig. 4). CX3CR1-GFP transgenic mice are often used in neuroscience studies to examine the roles of microglia in the brain. However, CX3CR1 (or fractalkine receptors) is instrumental in leukocyte adhesion and motility, with expression in neutrophils, monocytes, and lymphocytes (B cells, T cells, natural killer cells). While some of the microglia and macrophages divide in the CNS, leukocyte infiltration into the sub-dural space can be seen as early as 12 hours post-implantation. These cells squeeze through the endothelial cells of the BBB to enter the CNS (Fig. 5). An increase in BBB leakage (dye leakage) during or immediately after cells passed through the BBB was not visible, however, additional research is necessary before concluding a causal relationship between leukocyte infiltration and BBB leakage. While these cells may accumulate on or below the dura and the dural sealant in BCI headcaps, the cytokines released from these surface leukocytes may greatly impact the tissue health below (Markwardt et al., 2013). Most current research has focused on the tissue reaction around Layer IV or Layer V of the cortex where the bulk cortical input and output neurons reside; however, the impact of the craniotomy related tissue reaction on the underlying brain tissue might be significant and needs to be emphasized.

Giant Cells—In addition to leukocyte infiltration, CX3CR1+ giant cells were also identified on the window and probe in all animals (Fig. 6). Large, oval and circular CX3CR1+ cells about 50μm in diameter were observed as early 2 weeks on probe shanks and Kwik-Sil (Fig. 6a and b). Cells on the Kwik-Sil persisted until at least three months whereas cells on the electrode shank were only discernable through the first month post implant. Upon explantation, cranial windows and probes were stained with Hoescht to label nuclei as well as antibodies directed to monocyes (Iba-1), reactive monocytes (ED-1), and fibroblast/macrophages (Vimentin). While we were not able to identify clear cellular morphology on explanted probes, we were able to identify nuclei patterns consistent with foreign body giant cells (FBGC), which present as large clusters of nuclei, and Langhans' or Touton's giant cells, which both contain nuclei arranged as a horseshoe or a ring around the cell body (Fig. 6c). These giant cells types were found in all tested samples (n=7) and they were found to adhere to the silicone elastomer with discernable cellular morphology (Fig. 6 d-f). Langhans' and Touton's cells are typically associated with chronic infections and

Author Manuscript Author Manuscript Author Manuscript Author Manuscript

necrosis of fatty tissue, respectively, but are both more generally the product of persistent inflammatory environments, which is typical of the environment surrounding an implanted neural device(Karumbaiah et al., 2012; Quinn and Schepetkin, 2009). With no other signs of infection, we believe the identification of Langhans' and Touton's giant cells do not indicate infection, but rather a typical chronic inflammatory host tissue response to a foreign body. FBGC are also expected in the presence of a chronically implanted foreign body. It is believed that the fusion of macrophages is done in attempt to degrade large, non-phagocytosable materials (Anderson, 2000).

Intravascular Dye Leakage—One interesting observation is that a bulk of the intravascular dye leakage in chronically implanted animals was on the surface of the brain. Intravascular sulfarhodamine101 (SR101) can be seen with high intensity above the surface of the brain (Fig. 7a). Below the surface of the brain, SR101 is localized to the blood vessels and immediately adjacent to the probe (Fig. 7b), where some vascularization can also be seen. The 3D reconstruction of the data greatly emphasizes that the observed leakage is on the surface of the brain (Fig. 7c). This leakage may be the result of vascular contributions from the dura or the bone where it was drilled during the craniotomy, while there is limited vascular leakage from the deeper tissue around the implant. Here the higher Z-axis resolution of TPM technology has provided more precise information than some other imaging modalities, such as fluorescence molecular tomography, in which the recorded BBB leakage signal can be the sum of signal above the brain tissue (in the craniotomy) and that in the brain tissue (Saxena et al., 2013). In this previous study, the intravascular dye leakage was attributed to BBB leakage. However, the chronic two-photon data collected with this preparation provides much higher resolution than FMT and enable the visualization of intravascular dye at different depths. This data suggests that more careful consideration may be necessary to de-coupling dye leakage from the craniotomy injury outside of the BBB (eg. bone) and BBB leakage. While this leakage pattern was observed in all animals examined, additional studies are necessary to control the craniotomy procedure between experimental groups as well as identifying the impact of different craniotomy sizes and procedure on implant performance.

Longer-term Chronic Imaging—TPM through the cranial window was clear through the three month endpoint in all of the 3 animals tested. Probe tips were clearly visible at all time points, with discernable morphology of surrounding monocytes and degree of probe encapsulation (Fig. 8). Analysis of the 3D projections of Z-stacks in one animal indicate growth of fibrous tissue from ~16 μm at Day 0 to 150 μm by Week 1, with a large presence of circular migrating microglia and macrophages. The tissue contracted to ~120 μm at Month 1 before returning to 150 μm by Month 2 and maintaining this thickness through the Month 3 end-point. Due to the size of small neutrophils and multinucliated giant cells, as well as differences cell-cell spacing, cell counting was not possible as a function of depth, nor did shallow region cell counting correlate with functional imaging depth. Extracellular matrix components and solutes in the CSF, which could not be visualized or quantified in the current method, may contribute to decreased imaging depths.

Author Manuscript Author Manuscript Author Manuscript Author Manuscript

Proliferation of dura mater/fibrous tissue following surgical intervention has been well documented with post-surgical epidural fibrosis, as well as in craniotomies with either no sealant or PEG or alginate based sealants (Masopust et al., 2009; Nunamaker and Kipke, 2010; Preul et al., 2003). It has also been reported that fibrous encapsulation of epidurally implanted silicone electrocorticography grids with no sealant can occur as quickly as one week, with fibrous tissue ultimately between 300-700 μm thick (Schendel et al., 2014). Consistent with Schendel et al.'s study, we saw limited bone regrowth into the craniotomy. This has also been reported in studies using silicone elastomer as a sealant, but not with PEG-based sealants, which encourage bone regrowth into large calvarial defects (Lutolf et al., 2003; Spitler and Gothard, 2008; Terella et al., 2010). Kwik-Sil is an optically clear, chemically stable, hydrophobic and dense material which inhibits cell infiltration and is not permissive for cell ingrowth. In contrast, hydrogel sealants can provide a scaffold that facilitate cell infiltration. It may be possible that the decreased number of cells in the craniotomy space leads to a decreased overall pro-inflammatory cytokines released. However, this will need to be more comprehensively studied in the future.

While multiphoton microscopy is limited to shallower regions of small animal models, advances in optics, such as regenerative amplification multiphoton microscopy (Mittmann et al., 2011), adaptive optics (Ji et al., 2010), multiphoton microscopy (Horton et al., 2013), liquid light guide technology, and a greater library of long wavelength proteins and dyes (red, far red, and infra-red) continue to push the boundaries of two-photon imaging depth. Most importantly, despite the presence of this fibrous tissue, we were still able to clearly resolve the entire neural probe with TPM. This method will not match the resolution of two-photon post mortem immunohistochemistry. However, it provides the ability to track the dynamic chronic tissue response, and provides a new means towards better understanding of cause and effect relationships between tissue responses and recording performance.

Conclusion

We have described a method to prepare a cranial window to longitudinally observe tissue reaction to an implanted neural probe for at least 3 months. Sealants limit cell infiltration into the craniotomy space, thereby limiting light scattering and improving window clarity over time. Swelling of hydrophilic sealants can disrupt probe performance by displacing brain tissue, while hydrophobic sealants allow cell adhesion and attract giant cells. Dural fibrosis appeared to stabilize after two months, and while it is unclear how the fibrosis layer affects device performance, it did not impede our ability to study the device with TPM. Despite these new challenges, the described method provides a valuable tool to evaluate the chronic inflammatory response and performance of new neural technologies. With this established method, it will be possible study the long term dynamic effects and side-effects of different intervention strategies such as biological camouflage coatings and controlled anti-inflammatory drug release (Azemi et al., 2011; Luo et al., 2011).

Supplementary Material

Refer to Web version on PubMed Central for supplementary material.

Author Manuscript Author Manuscript Author Manuscript Author Manuscript

Acknowledgements

This project was financially supported by NIH R01 (Grant 5R01NS062019, 1R01NS089688, and 1R01NS094396), NIH K01 (Grant 1K01NS066131) and the Alzheimer's Association. The authors also like to thank Wai-Ying Wendy Yau for assistance with agarose windows.

References

Anderson JM. Multinucleated giant cells. Current opinion in hematology. 2000; 7:40–7. [PubMed: 10608503]

Azemi E, Lagenaur CF, Cui XT. The surface immobilization of the neural adhesion molecule L1 on neural probes and its effect on neuronal density and gliosis at the probe/tissue interface. Biomaterials. 2011; 32:681–92. [PubMed: 20933270]

Barrese JC, Rao N, Paroo K, Triebwasser C, Vargas-Irwin C, Franquemont L, Donoghue JP. Failure mode analysis of silicon-based intracortical microelectrode arrays in non-human primates. Journal of Neural Engineering. 2013; 10:066014. [PubMed: 24216311]

Bell RD, Winkler EA, Sagare AP, Singh I, LaRue B, Deane R, Zlokovic BV. Pericytes control key neurovascular functions and neuronal phenotype in the adult brain and during brain aging. Neuron. 2010; 68:409–27. [PubMed: 21040844]

Collinger JL, Wodlinger B, Downey JE, Wang W, Tyler-Kabara EC, Weber DJ, McMorland AJ, Velliste M, Boninger ML, Schwartz AB. High-performance neuroprosthetic control by an individual with tetraplegia. Lancet. 2012; 381(9866):557–64. [PubMed: 23253623]

Davalos D, Grutzendler J, Yang G, Kim JV, Zuo Y, Jung S, Littman DR, Dustin ML, Gan WB. ATP mediates rapid microglial response to local brain injury in vivo. Nature neuroscience. 2005; 8:752–8. [PubMed: 15895084]

Escamilla-Mackert T, Langhals NB, Kozai TDY, Kipke DR. Insertion of a three dimensional silicon microelectrode assembly through a thick meningeal membrane. Conf Proc IEEE Eng Med Biol Soc. 2009; 2009:1616–8. [PubMed: 19964007]

Freire MA, Morya E, Faber J, Santos JR, Guimaraes JS, Lemos NA, Sameshima K, Pereira A, Ribeiro S, Nicolelis MA. Comprehensive analysis of tissue preservation and recording quality from chronic multielectrode implants. PLoS One. 2011; 6:e27554. [PubMed: 22096594]

Gage GJ, Stoetzner CR, Wiltschko AB, Berke JD. Selective activation of striatal fast-spiking interneurons during choice execution. Neuron. 2010; 67:466–79. [PubMed: 20696383]

Ganguly K, Carmena JM. Emergence of a stable cortical map for neuroprosthetic control. PLoS Biol. 2009; 7:e1000153. [PubMed: 19621062]

Gilgunn PJ, Khilwani R, Kozai TDY, Weber DJ, Cui XT, Erdos G, Ozdoganlar OB, Fedder GK. An ultra-compliant, scalable neural probes with molded biodissolvable delivery vehicle. Micro Electro Mechanical Systems (MEMS), 2012 IEEE 25th International Conference on, 2012. 2012:56–9.

Gilgunn PJ, Xiao Chuan O, Flesher SN, Schwartz AB, Gaunt RA. Structural analysis of explanted microelectrode arrays. Neural Engineering (NER), 2013 6th International IEEE/EMBS Conference on. 2013:719–22.

Guitchounts G, Markowitz JE, Liberti WA, Gardner TJ. A carbon-fiber electrode array for long-term neural recording. J Neural Eng. 2013; 10:046016. [PubMed: 23860226]

Hochberg LR, Bacher D, Jarosiewicz B, Masse NY, Simeral JD, Vogel J, Haddadin S, Liu J, Cash SS, van der Smagt P, Donoghue JP. Reach and grasp by people with tetraplegia using a neurally controlled robotic arm. Nature. 2012; 485:372–5. [PubMed: 22596161]

Horton NG, Wang K, Kobat D, Clark CG, Wise FW, Schaffer CB, Xu C. In vivo three-photon microscopy of subcortical structures within an intact mouse brain. Nat Photon. 2013; 7:205–9.

Jaquins-Gerstl A, Shu Z, Zhang J, Liu Y, Weber SG, Michael AC. Effect of dexamethasone on gliosis, ischemia, and dopamine extraction during microdialysis sampling in brain tissue. Analytical Chemistry. 2011; 83:7662–7. [PubMed: 21859125]

Ji N, Milkie DE, Betzig E. Adaptive optics via pupil segmentation for high-resolution imaging in biological tissues. Nat Methods. 2010; 7:141–7. [PubMed: 20037592]

Author Manuscript Author Manuscript Author Manuscript Author Manuscript

Karumbaiah L, Norman SE, Rajan NB, Anand S, Saxena T, Betancur M, Patkar R, Bellamkonda RV. The upregulation of specific interleukin (IL) receptor antagonists and paradoxical enhancement of neuronal apoptosis due to electrode induced strain and brain micromotion. Biomaterials. 2012; 33:5983–96. [PubMed: 22681976]

Kim BJ, Washabaugh EP, Meng E. Annealing effects on flexible multi-layered parylene-based sensors. Micro Electro Mechanical Systems (MEMS), 2014 IEEE 27th International Conference on. 2014:825–8.

Kozai, T.; Alba, N.; Zhang, H.; Kotov, N.; Gaunt, R.; Cui, X. Nanostructured coatings for improved charge delivery to neurons.. In: Vittorio, MD.; Martiradonna, L.; Assad, J., editors. Nanotechnology and neuroscience: nano-electronic, photonic and mechanical neuronal interfacing. Springer New York; New York, NY: 2014a. p. 71-134.

Kozai TDY, Catt K, Du Z, Kyounghwan N, Srivannavit O, Haque RM, Seymour JP, Yoon E, Cui XT. Chronic in vivo evaluation of PEDOT/CNT for stable neural recordings. IEEE Trans Biomed Eng. 2015a; 63:111–119. [PubMed: 26087481]

Kozai TDY, Catt K, Li X, Gugel ZV, Olafsson VT, Vazquez AL, Cui XT. Mechanical failure modes of chronically implanted planar silicon-based neural probes for laminar recording. Biomaterials. 2015b; 37:25–39. [PubMed: 25453935]

Kozai TDY, Du Z, Gugel ZV, Smith MA, Chase SM, Bodily LM, Caparosa EM, Friedlander RM, Cui XT. Comprehensive chronic laminar single-unit, multi-unit, and local field potential recording performance with planar single shank electrode arrays. Journal of Neuroscience Methods. 2015c; 242:15–40. [PubMed: 25542351]

Kozai TDY, Gugel Z, Li X, Gilgunn PJ, Khilwani R, Ozdoganlar OB, Fedder GK, Weber DJ, Cui XT. Chronic tissue response to carboxymethyl cellulose based dissolvable insertion needle for ultra-small neural probes. Biomaterials. 2014b; 35:9255–68. [PubMed: 25128375]

Kozai TDY, Jaquins-Gerstl A, Vazquez AL, Michael AC, Cui XT. Brain Tissue Responses to Neural Implants Impact Signal Sensitivity and Intervention Strategies. ACS Chemical Neuroscience. 2015d; 6:48–67. [PubMed: 25546652]

Kozai TDY, Langhals NB, Patel PR, Deng X, Zhang H, Smith KL, Lahann J, Kotov NA, Kipke DR. Ultrasmall implantable composite microelectrodes with bioactive surfaces for chronic neural interfaces. Nature materials. 2012a; 11:1065–73. [PubMed: 23142839]

Kozai TDY, Li X, Bodily LM, Caparosa EM, Zenonos GA, Carlisle DL, Friedlander RM, Cui XT. Effects of caspase-1 knockout on chronic neural recording quality and longevity: Insight into cellular and molecular mechanisms of the reactive tissue response. Biomaterials. 2014c; 35:9620–34. [PubMed: 25176060]

Kozai TDY, Marzullo TC, Hooi F, Langhals NB, Majewska AK, Brown EB, Kipke DR. Reduction of neurovascular damage resulting from microelectrode insertion into the cerebral cortex using in vivo two-photon mapping. J Neural Eng. 2010; 7:046011. [PubMed: 20644246]

Kozai TDY, Vazquez AL, Weaver CL, Kim SG, Cui XT. In vivo two photon microscopy reveals immediate microglial reaction to implantation of microelectrode through extension of processes. J Neural Eng. 2012b; 9:066001. [PubMed: 23075490]

Ludwig KA, Uram JD, Yang J, Martin DC, Kipke DR. Chronic neural recordings using silicon microelectrode arrays electrochemically deposited with a poly(3,4-ethylenedioxythiophene) (PEDOT) film. J Neural Eng. 2006; 3:59–70. [PubMed: 16510943]

Luo X, Matranga C, Tan S, Alba N, Cui XT. Carbon nanotube nanoreservior for controlled release of anti-inflammatory dexamethasone. Biomaterials. 2011; 32:6316–23. [PubMed: 21636128]

Lutolf M, Hubbell J. Synthesis and physicochemical characterization of end-linked poly (ethylene glycol)-co-peptide hydrogels formed by Michael-type addition. Biomacromolecules. 2003; 4:713–22. [PubMed: 12741789]

Lutolf MP, Weber FE, Schmoekel HG, Schense JC, Kohler T, Müller R, Hubbell JA. Repair of bone defects using synthetic mimetics of collagenous extracellular matrices. Nature biotechnology. 2003; 21:513–8.

Markwardt NT, Stokol J, Rennaker RL Ii. Sub-meninges implantation reduces immune response to neural implants. Journal of Neuroscience Methods. 2013; 214:119–25. [PubMed: 23370311]

Author Manuscript Author Manuscript Author Manuscript Author Manuscript

Masamoto K, Tomita Y, Toriumi H, Aoki I, Unekawa M, Takuwa H, Itoh Y, Suzuki N, Kanno I. Repeated longitudinal in vivo imaging of neuro-glio-vascular unit at the peripheral boundary of ischemia in mouse cerebral cortex. Neuroscience. 2012; 212:190–200. [PubMed: 22516017]

Masopust V, Häckel M, Netuka D, Bradác O, Rokyta R, Vrabec M. Postoperative epidural fibrosis. Clin J Pain. 2009; 25:600–6. [PubMed: 19692802]

Mittmann W, Wallace DJ, Czubayko U, Herb JT, Schaefer AT, Looger LL, Denk W, Kerr JN. Two-photon calcium imaging of evoked activity from L5 somatosensory neurons in vivo. Nat Neurosci. 2011; 14:1089–93. [PubMed: 21743473]

Nunamaker EA, Kipke DR. An alginate hydrogel dura mater replacement for use with intracortical electrodes. Journal of Biomedical Materials Research Part B: Applied Biomaterials. 2010; 95:421–9.

Potter KA, Buck AC, Self WK, Callanan ME, Sunil S, Capadona JR. The effect of resveratrol on neurodegeneration and blood brain barrier stability surrounding intracortical microelectrodes. Biomaterials. 2013; 34:7001–15. [PubMed: 23791503]

Prasad A, Xue QS, Dieme R, Sankar V, Mayrand RC, Nishida T, Streit WJ, Sanchez JC. Abiotic-biotic characterization of Pt/Ir microelectrode arrays in chronic implants. Front Neuroeng. 2014; 7:2. [PubMed: 24550823]

Prasad A, Xue QS, Sankar V, Nishida T, Shaw G, Streit WJ, Sanchez JC. Comprehensive characterization and failure modes of tungsten microwire arrays in chronic neural implants. J Neural Eng. 2012; 9:056015. [PubMed: 23010756]

Preul MC, Bichard WD, Muench TR, Spetzler RF. Toward optimal tissue sealants for neurosurgery: use of a novel hydrogel sealant in a canine durotomy repair model. Neurosurgery. 2003; 53:1189–99. [PubMed: 14580287]

Quinn MT, Schepetkin IA. Role of NADPH oxidase in formation and function of multinucleated giant cells. Journal of innate immunity. 2009; 1:509–26. [PubMed: 20375608]

Rennaker RL, Miller J, Tang H, Wilson DA. Minocycline increases quality and longevity of chronic neural recordings. Journal of Neural Engineering. 2007; 4:L1–5. [PubMed: 17409469]

Rousche PJ, Normann RA. Chronic recording capability of the Utah Intracortical Electrode Array in cat sensory cortex. J Neurosci Methods. 1998; 82:1–15. [PubMed: 10223510]

Sankar V, Patrick E, Dieme R, Sanchez JC, Prasad A, Nishida T. Electrode impedance analysis of chronic tungsten microwire neural implants: understanding abiotic vs. biotic contributions. Front Neuroeng. 2014; 7:13. [PubMed: 24847248]

Saxena T, Karumbaiah L, Gaupp EA, Patkar R, Patil K, Betancur M, Stanley GB, Bellamkonda RV. The impact of chronic blood-brain barrier breach on intracortical electrode function. Biomaterials. 2013

Schendel AA, Nonte MW, Vokoun C, Richner TJ, Brodnick SK, Atry F, Frye S, Bostrom P, Pashaie R, Thongpang S, Eliceiri KW, Williams JC. The effect of micro-ECoG substrate footprint on the meningeal tissue response. J Neural Eng. 2014; 11:046011. [PubMed: 24941335]

Spitler KM, Gothard KM. A removable silicone elastomer seal reduces granulation tissue growth and maintains the sterility of recording chambers for primate neurophysiology. J Neurosci Methods. 2008; 169:23–6. [PubMed: 18241928]

Stensaas SS, Stensaas LJ. Histopathological evaluation of materials implanted in the cerebral cortex. Acta Neuropathol (Berl). 1978; 41:145–55. [PubMed: 636844]

Stoetzner CR, Pettibone JR, Berke JD. State-dependent plasticity of the corticostriatal pathway. Neuroscience. 2010; 165:1013–8. [PubMed: 19932155]

Terella A, Mariner P, Brown N, Anseth K, Streubel S-O. Repair of a calvarial defect with biofactor and stem cell–embedded polyethylene glycol scaffold. Archives of facial plastic surgery. 2010; 12:166–71. [PubMed: 20479432]

Tibbitt MW, Anseth KS. Hydrogels as extracellular matrix mimics for 3D cell culture. Biotechnol Bioeng. 2009; 103:655–63. [PubMed: 19472329]

Turner JN, Shain W, Szarowski DH, Andersen M, Martins S, Isaacson M, Craighead H. Cerebral astrocyte response to micromachined silicon implants. Exp Neurol. 1999; 156:33–49. [PubMed: 10192775]

Author Manuscript Author Manuscript Author Manuscript Author Manuscript

Wake H, Moorhouse AJ, Jinno S, Kohsaka S, Nabekura J. Resting microglia directly monitor the functional state of synapses in vivo and determine the fate of ischemic terminals. The Journal of neuroscience : the official journal of the Society for Neuroscience. 2009; 29:3974–80. [PubMed: 19339593]

Ware T, Simon D, Liu C, Musa T, Vasudevan S, Sloan A, Keefer EW, Rennaker RL 2nd, Voit W. Thiol-ene/acrylate substrates for softening intracortical electrodes. J Biomed Mater Res B Appl Biomater. 2014; 102:1–11. [PubMed: 23666562]

Williams JC, Rennaker RL, Kipke DR. Long-term neural recording characteristics of wire microelectrode arrays implanted in cerebral cortex. Brain Res Brain Res Protoc. 1999; 4:303–13. [PubMed: 10592339]

Author Manuscript Author Manuscript Author Manuscript Author Manuscript

Highlights

- silastic sealants limit cell infiltration into the craniotomy and improve image clarity
- low concentration hydrogel sealants failed to prevent cell infiltration
- high concentration hydrogel displaced brain tissue and disrupted probe performance.
- CX3CR1+ giant cells were identified on windows and probes
- BBB dye leakage was greatest in the craniotomy on the outside of the dura matter

Author Manuscript Author Manuscript Author Manuscript Author Manuscript

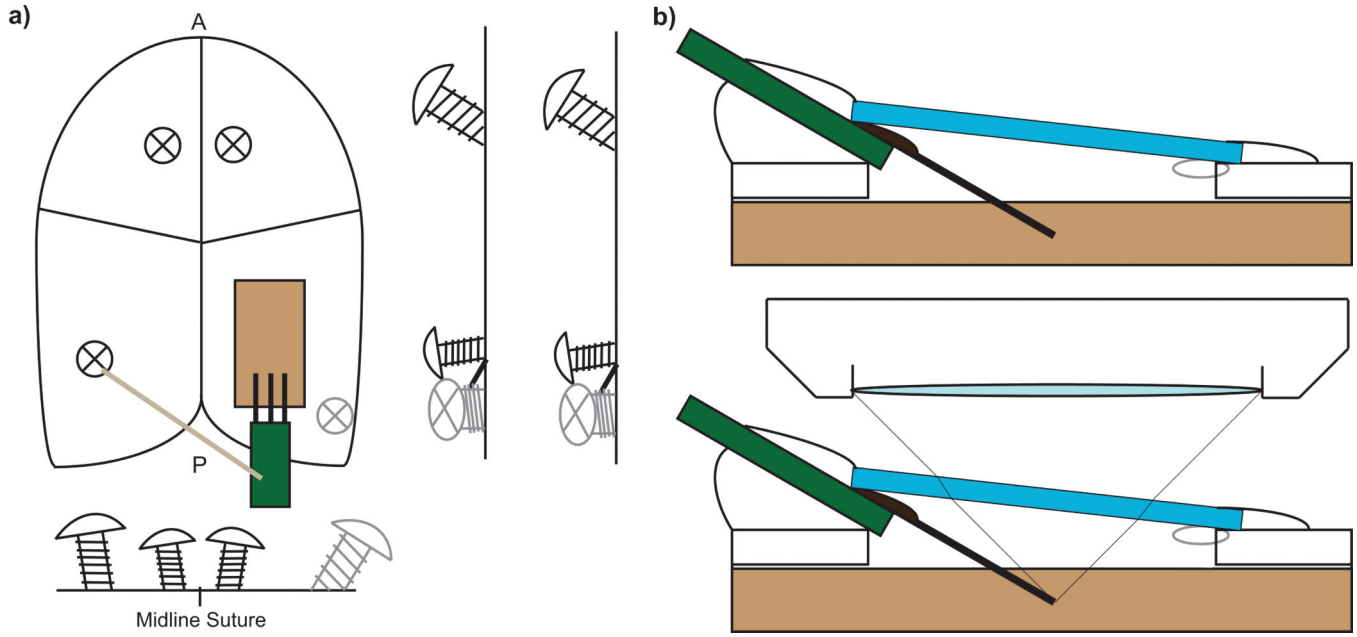

Figure 1.

Scheme for Chronic multiphoton imaging setup. **a)** Four bone screws are used to anchor the probe and imaging window as well as a well created for a water emersion microscope lens. **b)** Coverslip windows are gently placed on the probe after filling the cranial space and then sealed. When filling it with aCSF, it is necessary to leave a small air bubble to prevent a leaky seal. Small air bubbles are solubilized in the CSF over the first 12 hours. Probes must be inserted at an angle to prevent collision with the microscope lens. **c)** Locations of the bone screws. **d)** Preliminary dental cement well. **e)** Craniotomy. **f)** Insertion of the electrode and securing of the reference/ground wire. **g)** Sealing the craniotomy with Kwik-Sil, coverslip, and dental cement.

Author Manuscript Author Manuscript Author Manuscript Author Manuscript

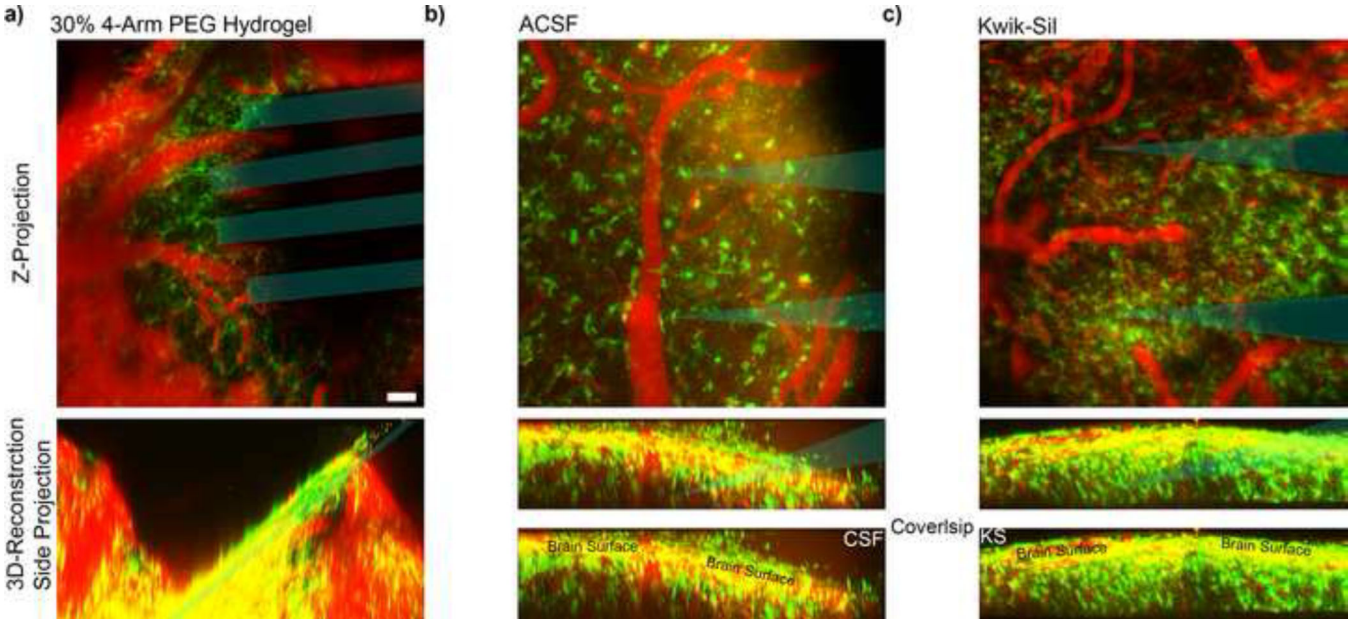

Figure 2.

Imaging through Early Chronic *In vivo* Cranial Windows. *Top:* Z-stack of entire imaging depth. *Bottom:* 3D-reconstruction of corresponding Z-stack viewed from the side. **a)** 30% covalently linked PEG hydrogel expanded an hour after sealing the cranial window, pushing down the brain tissue and probe. **b)** Cranial window sealed after being filled with aCSF. 48 hours after surgery, increased CX3CR1+ cells can be seen crawling on the dura and the window surface. **c)** Kwik-Sil (KS) minimizes CX3CR1+ cells from infiltrating the space between the dura and coverslip, leading to brighter signal from deeper tissue. Blue indicates probe track. Scale = 100 μm.

Author Manuscript Author Manuscript Author Manuscript Author Manuscript

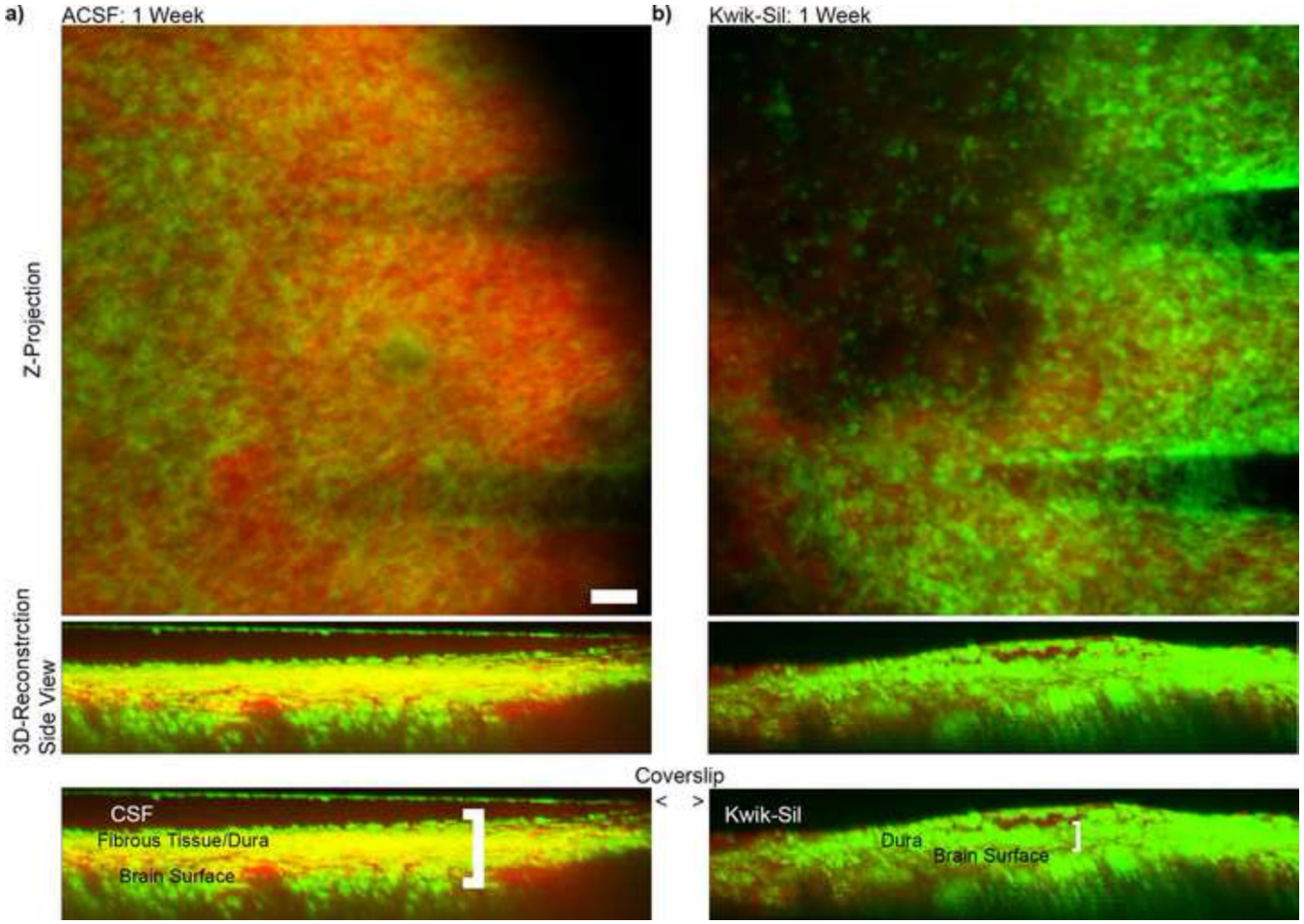

Figure 3.

Imaging through *In vivo* Cranial Window One Week Post-Implant. The fibrous CX3CR1+ tissue (green signal) on the surface of the brain is much greater in **a)** aCSF filled window compared to **b)** Kwik-Sil filled window. Due to the increased thickness of these cell layers, the effective imaging depth of the cortex is much less in aCSF filled windows. SR101 was administered to label the vasculature (red signal). Scale = 100 μm. Note: In the 3D reconstruction of (a), $CX3CR1^{+}$ cells can also be seen on the coverslip window.

Author Manuscript Author Manuscript Author Manuscript Author Manuscript

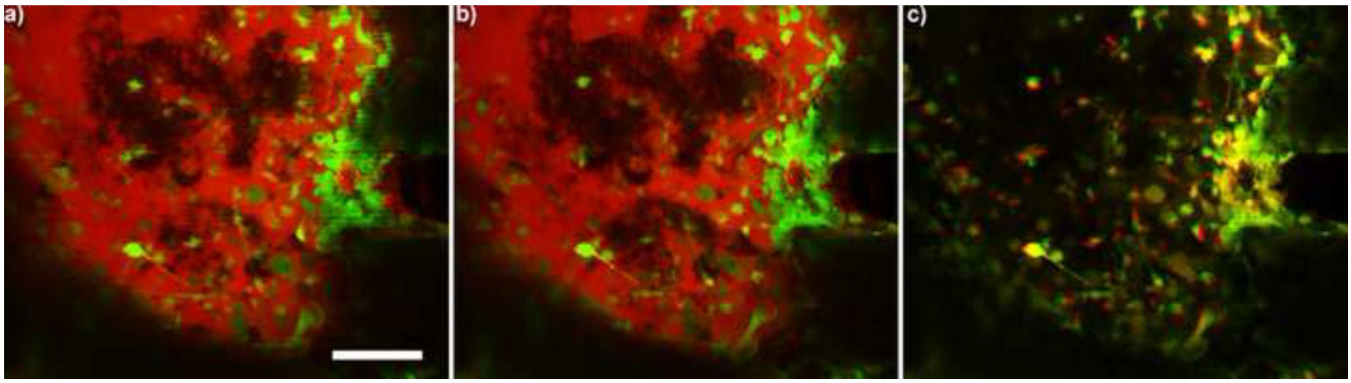

Figure 4.

$CX3CR1^{+}$ cells (green) migrating and encapsulating the window at **a)** 0 and **b)** 3 min. Dye in the craniotomy (red) also highlight unlabeled cells. **c)** Movement between the first three minutes are shown as an overlay. Red indicates where cells were at time 0, while green shows where cells moved to after 3 min. Yellow cells did not move during the imaging period. Time series was recorded 1 week post implant. Scale = 100 μm.

Author Manuscript Author Manuscript Author Manuscript Author Manuscript

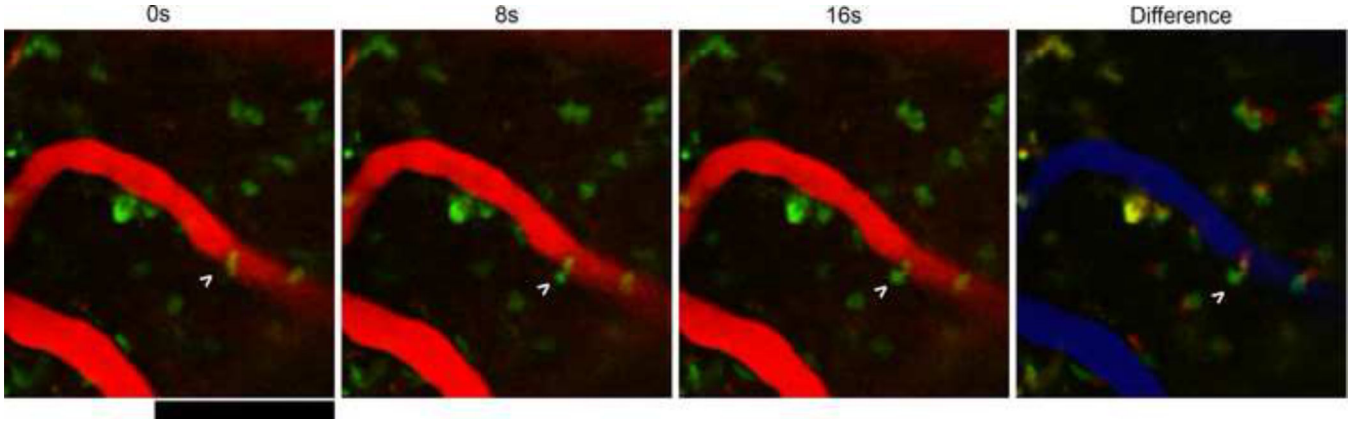

Figure 5.

$CX3CR1^{+}$ cell infiltration into imaging area. Arrow indicates cell in the BBB squeezing through the endothelium in to the CNS over 16 seconds. Difference shows 0s in red, 16s in green, and BBB in blue. Scale = 100 μm.

Author Manuscript Author Manuscript Author Manuscript Author Manuscript

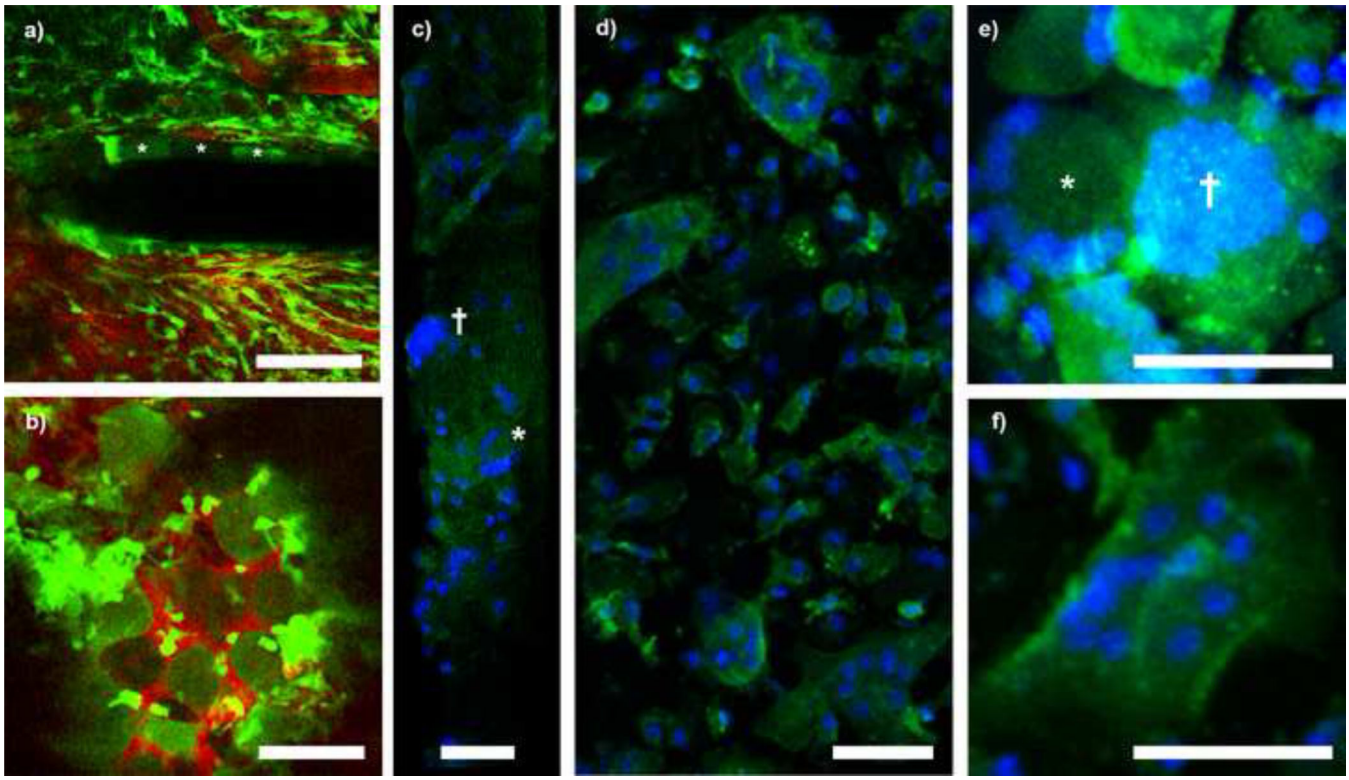

Figure 6.

Foreign body giant cell encapsulation of neural probe and Kwik-Sil at 1 month post implant. **A)** Large, oval CX3CR1^{+} cells encapsulated the device with morphology distinct from parenchymal microglia or meningeal macrophages. Cells denoted with asterisks. **B)** Unidentified round cells also adhered to the Kwik-Sil. **C)** Explanted electrodes show nuclei patterns (blue, Hoescht stain) consistent with FBGC (†) and Langhans' giant cells (*). **D)** Explanted Kwik-Sil with adherent giant cells (Blue: Hoescht; Green: Iba-1). **E-F)** Identification of FBCG (†)Langhans' (*), and Touton's giant cells (E) on Kwik-Sil (Blue: Hoescht; Green: Iba1). All scale bars are 50 μm.

Author Manuscript
Author Manuscript
Author Manuscript
Author Manuscript

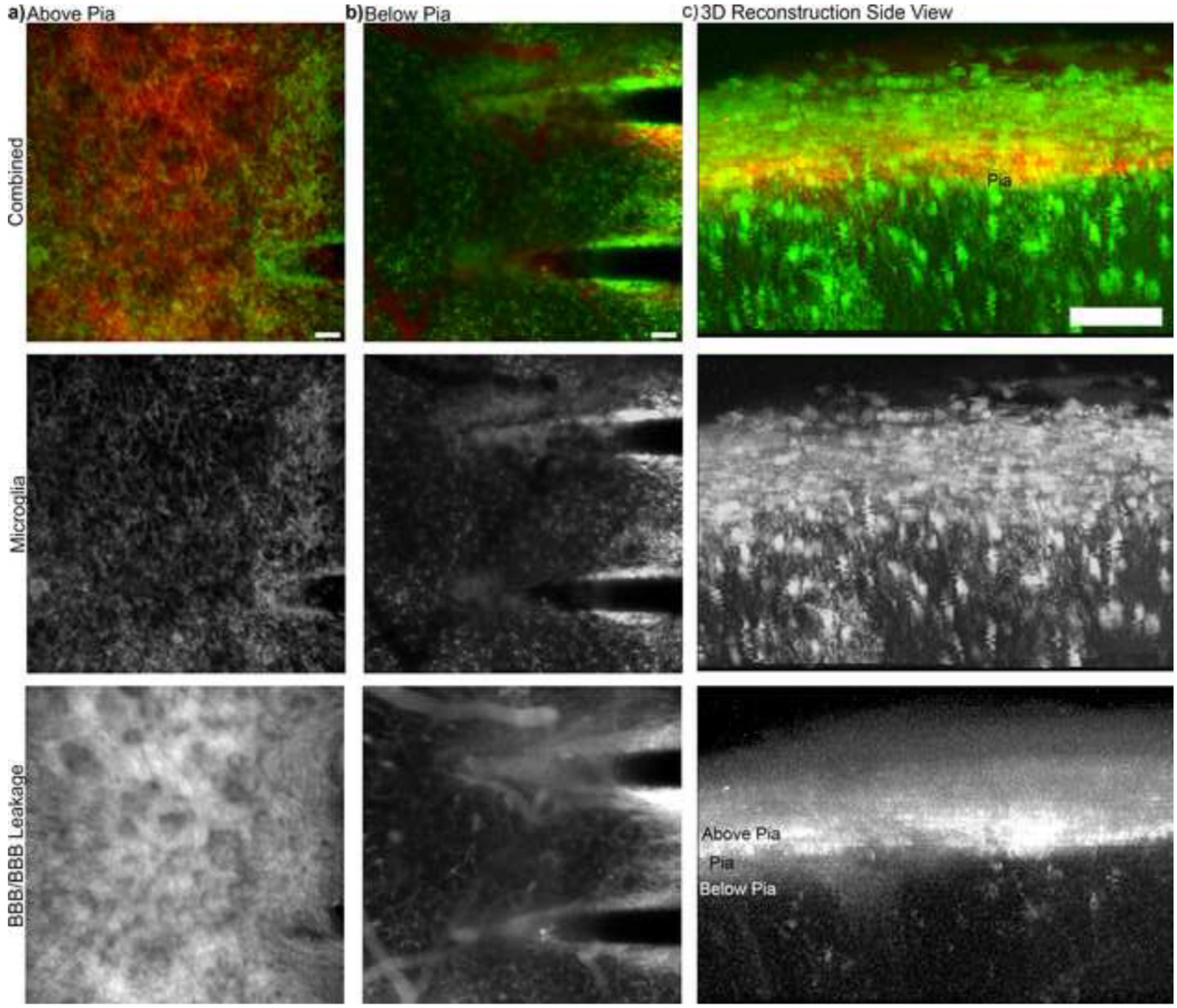

Figure 7.

BBB integrity and BBB Leakage. **a)** Z-stack of 100 μm above the pia. Substantial BBB leakage can be observed as indicated by SR101 leakage. **b)** Z-stack of 100 μm below the pia. Intravascular SR101 can be seen confined to the blood vessels and immediately adjacent to the probes, which also include additional vascular features. **c)** 3D-reconstruction side view emphasizes that BBB leakage is predominately above the brain and leakage is relatively dramatically reduced in the tissue.

Author Manuscript Author Manuscript Author Manuscript Author Manuscript

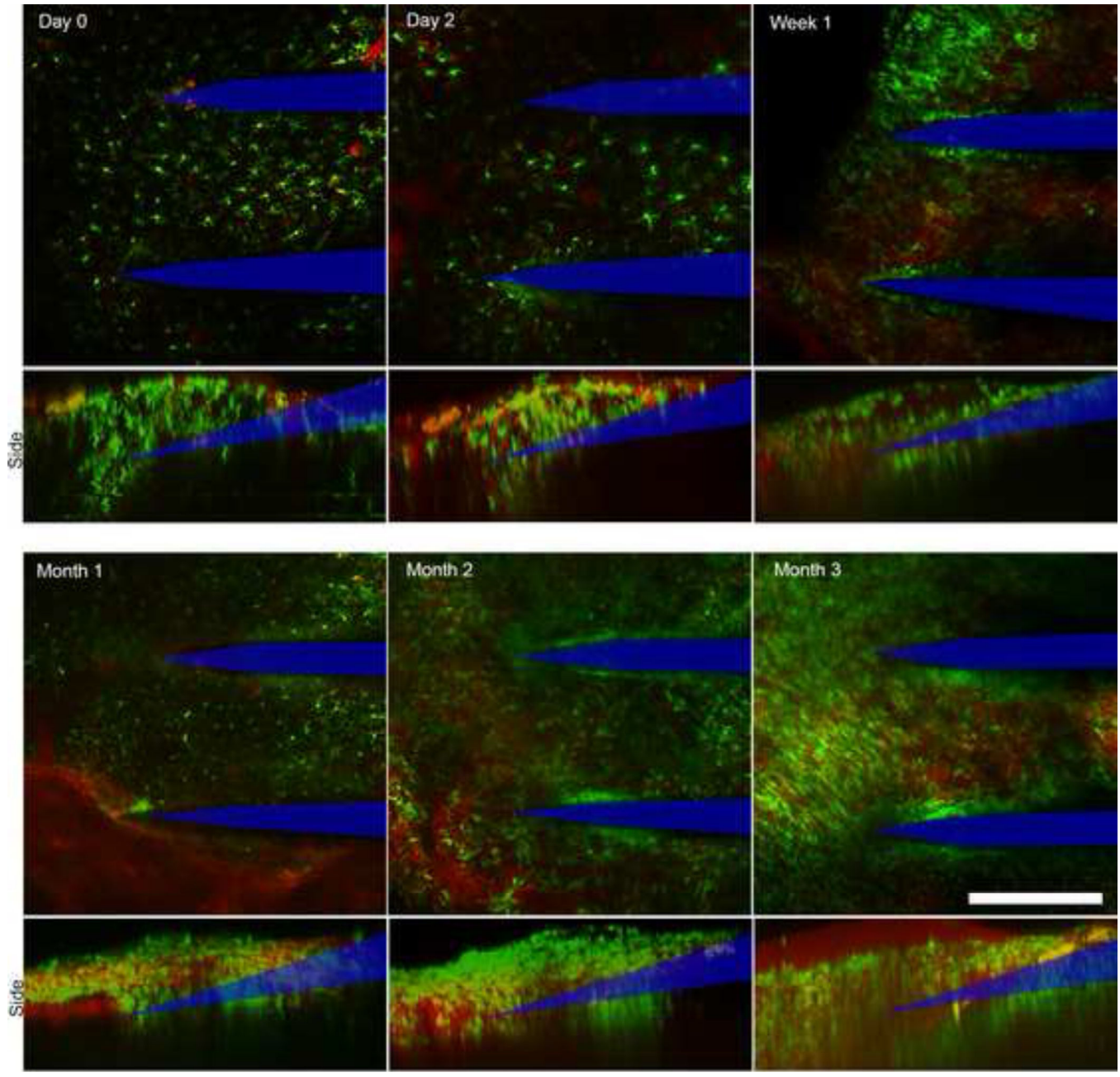

Figure 8.

Imaging through *in vivo* cranial window over three months. Probe tips observable through tissue at all time points, with clear morphology of surrounding monocytes. Bottom panels: 3D projections of Z-stacks reveal growth of fibrous tissue at the cortical surface (neural probe profile denoted by blue line). Scale bar = 150 μm.